Investigating Fluorescence Quenching of ZnS Quantum Dots by Silver Nanoparticles

Amit Jaiswal · Pallab Sanpui · Arun Chattopadhyay · Siddhartha Sankar Ghosh

Abstract Water dispersible zinc sulfide quantum dots (ZnS QDs) with an average diameter of 2.9 nm were synthesized in an environment friendly method using chitosan as stabilizing agent. These nanocrystals displayed characteristic absorption and emission spectra having an absorbance edge at 300 nm and emission maxima ($\lambda_{emission}$) at 427 nm. Citrate-capped silver nanoparticles (Ag NPs) of ca. 37-nm diameter were prepared by modified Turkevich process. The fluorescence of ZnS QDs was significantly quenched in presence of Ag NPs in a concentration-dependent manner with K_{sv} value of 9×10^9 M^{-1}. The quenching mechanism was analyzed using Stern–Volmer plot which indicated mixed nature of quenching. Static mechanism was evident from the formation of electrostatic complex between positively charged ZnS QDs and negatively charged Ag NPs as confirmed by absorbance study. Due to excellent overlap between ZnS QDs emission and surface plasmon resonance band of Ag NPs, the role of energy transfer process as an additional quenching mechanism was investigated by time-resolved fluorescence measurements. Time-correlated single-photon counting study demonstrated decrease in average lifetime of ZnS QDs fluorescence in presence of Ag NPs. The corresponding Förster distance for the present QD–NP pair was calculated to be 18.4 nm.

Keyword ZnS QDs · Ag NPs · Fluorescence quenching · Energy transfer

A. Jaiswal · S. S. Ghosh
Department of Biotechnology, Indian Institute
of Technology Guwahati,
Guwahati-39, Assam, India

P. Sanpui · A. Chattopadhyay (✉) · S. S. Ghosh (✉)
Centre for Nanotechnology, Indian Institute
of Technology Guwahati,
Guwahati-39, Assam, India
e-mail: arun@iitg.ernet.in

S. S. Ghosh
e-mail: sghosh@iitg.ernet.in

A. Chattopadhyay
Department of Chemistry, Indian Institute
of Technology Guwahati,
Guwahati-39, Assam, India

Introduction

Quantum dots (QDs) are inorganic semiconductor nanocrystals with remarkable optoelectronic properties originated from quantum confinement of the electronic motion, otherwise unavailable in either discrete atoms or bulk materials [1–3]. QDs have several advantages over conventional organic fluorophores because of their excellent resistance to photobleaching and optical properties tunable by size and material composition [4]. Most importantly, the broad absorption with narrow emission spectra of QDs makes them potential candidate for multiplex applications in bio-imaging as well as bio-tagging [1, 3]. In recent years, the extraordinary photophysical properties of QDs have been successfully exploited in various fields such as optoelectronic devices, imaging, as well as biodiagnostics [3, 5–7]. Various sensing application has been developed based on the quenching of QDs fluorescence by metal nanoparticles or other molecules [8, 9]. QDs can also act as efficient energy transfer donors or acceptors in fluorescence resonance energy transfer (FRET)-based applications [10, 11]. Several bioanalysis formats like molecular beacons, TaqMan probes, and immunoassays have been developed based on either quenching or FRET of QDs [1, 11].

In the last few years, a great deal of research—theoretical as well as experimental—has been carried out to understand the influence of metal surface on the emission properties of fluorophore [12–14]. A fluorophore near a metal film or metal nanoparticles (NPs) has been reported to show a varied degree of fluorescence depending on the distance between the metal surface and fluorophore [15, 16]. However, the exact mechanism of differential fluorescence exhibited by a fluorophore near a metal surface is still to be understood completely. In this regard, the fluorescent enhancement of conventional fluorophore or QDs in presence of silver nanoparticles (Ag NPs) has been well studied [17, 18]. However, there are only few reports where Ag NPs have been used as an efficient quencher of the fluorophore [19, 20]. Tay et al. has showed that the photoluminescence of surface-functionalized Si was quenched by Ag NPs [21]. Recently it has been reported that Ag NPs quenched the fluorescence of 1,4-dihydroxy-2,3-dimethyl-9,10-anthraquinone depending upon the particle size [22]. Ag NPs have been reported to act as enhancer of FRET efficiency, where hybridization of the donor-labeled oligonucleotide with the acceptor-labeled complimentary strand on Ag NP surface led to larger Förster distance. Zhang et al. showed that the FRET efficiency between cy5 and cy5.5 on the surface of Ag NPs was increased with particle size [23]. The report suggested that the conventional Förster distance can be increased to 75% by varying the particle size of the Ag NPs. However, the length scale for detecting dynamic changes in FRET-based methods is limited to a distance of <10 nm by the nature of the dipole–dipole mechanism. On the other hand, Yun et al. [24] reported that the energy transfer from a dipole to a nanometal surface (nanometal surface energy transfer, NSET) follows a $1/R^4$ distance dependence and the traditional Förster distance can be increased up to the range of 22 nm. The quenching property of Ag NPs in FRET or NSET applications could stem from their plasmon resonance in the visible range which makes them strong absorbers with large extinction coefficients [25]. The development of long-range FRET is, therefore, critical to investigate the biological multi-component systems such as ribosomes or various nucleo-protein complexes [24].

In this paper, we report the fluorescence quenching of zinc sulfide quantum dots (ZnS QDs) by Ag NPs. Ag NPs were observed to act as an efficient quencher of ZnS QDs, exhibiting K_{sv} value approaching 9×10^9 M^{-1}. The corresponding Stern–Volmer plot indicated mixed quenching mechanism to be involved in the present study. The static quenching was investigated by absorbance study as well as regaining of quenched fluorescence on salt addition. The energy transfer process involved in the present quenching was studied by time-resolved fluorescence spectroscopy.

Experimental

Materials

Zinc acetate dihydrate [Zn(CH$_3$COO)$_2$, 2H$_2$O], sodium sulfide [Na$_2$S], trisodium citrate, silver nitrate, and acetic acid (glacial, 99–100%) were purchased from Merck India Ltd, Mumbai, India. Chitosan (high MW, >75% deacety-lated) was obtained from Sigma–Aldrich Chemical Pvt. Ltd., Kolkata, India. All chemicals employed were of AR grade and were used as received without further purification. Milli-Q ultra pure water (>18 MΩ cm, Millipore) was used in all experiment.

Synthesis of Chitosan-Stabilized ZnS QDs

The synthesis of chitosan-stabilized ZnS QDs was carried out using a modified inorganic wet-chemical synthesis method reported by Warad et al. [26]. Briefly, 21 mg zinc acetate (0.01 M) was added to 9 ml of 0.05% (w/v) chitosan solution under constant stirring and heated at 80 °C for 15 min. After cooling to room temperature, 1 mL of freshly prepared 16 mg mL^{-1} sodium sulfide was added dropwise to the mixture in an ice bath with continuous stirring. This resulted in the formation of a milky white suspension without any sedimentation for more than 24 h, indicating the synthesis of ZnS nanocrystals. The as-prepared colloidal solution of ZnS QDs was ultrasonicated to remove the dissolved gases, if any. Next, ZnS QDs were characterized by transmission electron microscopy (TEM) by a JEOL 2100 UHR-TEM instrument. Five microliters of ZnS QDs solution was drop-cast on carbon-coated copper grids and subsequently air-dried before TEM analysis. X-ray diffraction (XRD) pattern were recorded with Brucker D8 Advanced X-ray diffraction measurement system, with Cu Kα source (λ=1.54 Å). UV-visible absorption spectra were recorded on a Varian Cary 100 spectrophotometer. Steady-state fluorescence intensity was measured using Jobin-Yvon Fluoromax-3 spectrofluorimeter at an excitation wavelength of 315 nm. Quantum yield of ZnS QDs were calculated according to Williams' method [27] using Rhodamine 101 as a reference (Q.Y.=100%) [28].

Synthesis of Citrate-Capped Ag NPs

Citrate-capped Ag NPs were prepared by a modified Turkevich method [29]. Briefly, 1 mM aqueous solution of AgNO$_3$ was heated until it started to boil. As the boiling started, sodium citrate (5 mM) was added to it. The color of the solution slowly turned yellow and then grayish yellow after 30 min of boiling, indicating formation of Ag NPs. The reaction was performed under refluxing condition to

avoid loss of water by evaporation during boiling. The solution was cooled to room temperature and kept for 1 day. In order to remove excess Ag^+ ions, if any, the Ag NPs solution was centrifuged at $13,000 \times g$ for 15 min and the pellet was washed for several times. Finally, the washed Ag NPs were resuspended in Milli-Q water and subsequently characterized by using UV-visible absorption spectroscopy (Varian Cary 100 spectrophotometer) and TEM (JEOL 2100 UHR-TEM instrument). The particle size determined by TEM analysis was used to calculate the concentration of Ag NPs.

Fluorescence Quenching of ZnS QDs by Ag NPs

The chitosan-stabilized ZnS QDs were diluted to 1.4 μM in Milli-Q water and different concentrations of citrate-capped Ag NPs were added to it. The pH of all the samples was 5.5. After 1 h of incubation, each sample was studied by steady state fluorescence as well as absorption spectroscopy. For all steady state fluorescence, measurement excitation was set at 315 nm and the fluorescence emission spectra were recorded in the wavelength range of 360–560 nm. For quenching experiments, the integrated fluorescence intensity in the abovementioned range was used to determine F_o/F since it gave a flat baseline free from Raman scatter. Time-resolved intensity decays of the ZnS QDs both in absence and presence of quencher were recorded using a Life Spec II spectrofluorimeter (Edinburgh Instrument). The sample was excited by PicoQuant 308 nm LED source, and the decay was measured in a time scale of 0.0488 ns/channel. The decay curves were analyzed by FAST software, provided by Edinburgh Instrument along with the fluorescence instrument.

Results and Discussion

As evident from the TEM image (Fig. 1a), the chitosan-stabilized ZnS QDs synthesized in the present study were nearly monodisperse and spherical in shape. The average particle size was found to be 2.9 nm from the corresponding particle size distribution shown in Fig. 1b. The high-resolution TEM (HRTEM) image shown in the inset of Fig. 1a, depicts the lattice-resolved structure of ZnS QDs. The UV-visible absorption spectrum (Fig. 1c) of the ZnS QDs showed absorption edge around 300 nm, considerably blue-shifted compared to that of bulk ZnS at 340 nm [30]. This shift in band gap can be explained by the effective mass approximation model with the particle in a box approach [31]. Based on the first order approximation of Brus equation [32], the relationship between the particle radius (r) and band gap E_g in ZnS nanocrystal [33] is given by

$$r(E_g) = \frac{0.32 - 2.9\sqrt{(E_g - 3.49)}}{2(3.50 - E_g)} \tag{1}$$

Using Eq. (1), the diameter of the ZnS nanocrystal (considering $E_g = 4.14$ eV) was calculated to be 3.14 nm which is in good agreement with TEM results. The extinction coefficient of ZnS QDs at 315 nm was estimated to be 3.3×10^5 $M^{-1}cm^{-1}$. The crystallinity of the ZnS QDs was confirmed by powder XRD analysis. The XRD pattern (Fig. 1d) consisted of characteristic peaks at 28.5°, 47.5°, and 56.5° corresponding to principal Bragg reflections in (111), (220), and (311) lattice planes, respectively, of bulk ZnS crystallizing in Wurtzite structure according to the JCPDS-ICDD database [34]. The quantum yield of ZnS QDs was calculated to be 9.5%.

Citrate-capped Ag NPs were prepared using a modified Turkevich process [29]. The TEM images revealed that the prepared Ag NPs are well-separated and mostly spheroid in shape. Selected area electron diffraction (SAED) pattern of the Ag NPs (inset of Fig. 2) indicated poly-crystalline nature of the NPs. The average particle size was determined to be 37 nm from the corresponding particle size distribution (inset Fig. 2). A strong surface plasmon resonance (SPR) band at 418 nm, characteristic of Ag NPs [35, 36], was observed in the corresponding UV-visible spectra. The extinction coefficient of citrate-capped Ag NPs at 418 nm was estimated to be 1×10^{10} $M^{-1}cm^{-1}$. It may be mentioned here that no significant emission was observed for the prepared Ag NPs at the excitation wavelength of 315 nm.

The effect of Ag NPs on the fluorescence properties of ZnS QDs was first investigated by steady state fluorescence spectroscopy. The fluorescence intensity of ZnS QDs in presence of different concentrations of Ag NPs was recorded and the results are shown in Fig. 3a. Figure 3a clearly shows that the fluorescence of ZnS QDs was efficiently quenched by Ag NPs in a concentration-dependent way. It may be mentioned here that no quenching of ZnS QDs fluorescence was observed in presence of citrate, indicating the Ag NPs to be solely responsible for quenching effect.

The fluorescence quenching was further analyzed using the well known Stern–Volmer equation [28]

$$\frac{F_0}{F} = 1 + K_{sv}[Q] \tag{2}$$

where, F_0 and F represents the integrated fluorescence intensity in absence and presence of quencher, respectively, K_{sv} is the Stern–Volmer quenching constant and $[Q]$ is the concentration of quencher. The corresponding Stern–Volmer plot (Fig. 3b) demonstrates the quenching in the present QD–NP pair is linear in the lower quencher concentration range (0–100 pM) with a K_{sv} value of 9×10^9 M^{-1}. The high K_{sv} value indicates the efficient

Fig. 1 **a** TEM image of ZnS QDs with HRTEM image (*inset*) showing lattice fringes. **b** Particle size distribution, **c** UV-visible spectra, and **d** XRD pattern of the corresponding ZnS QDs
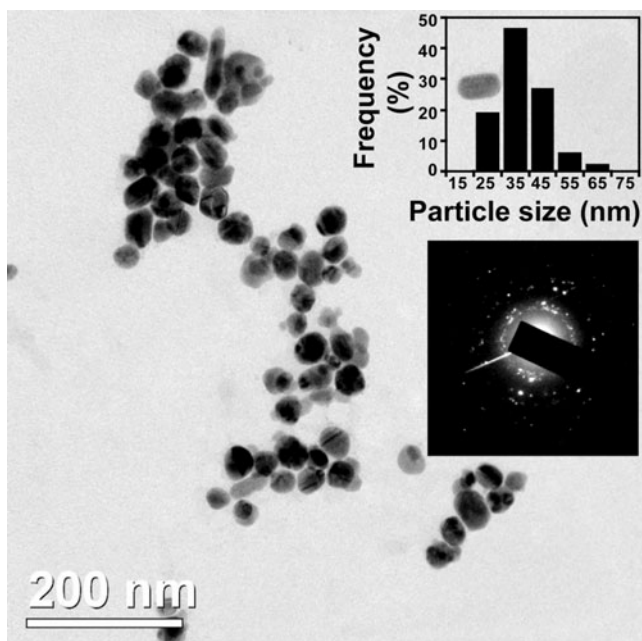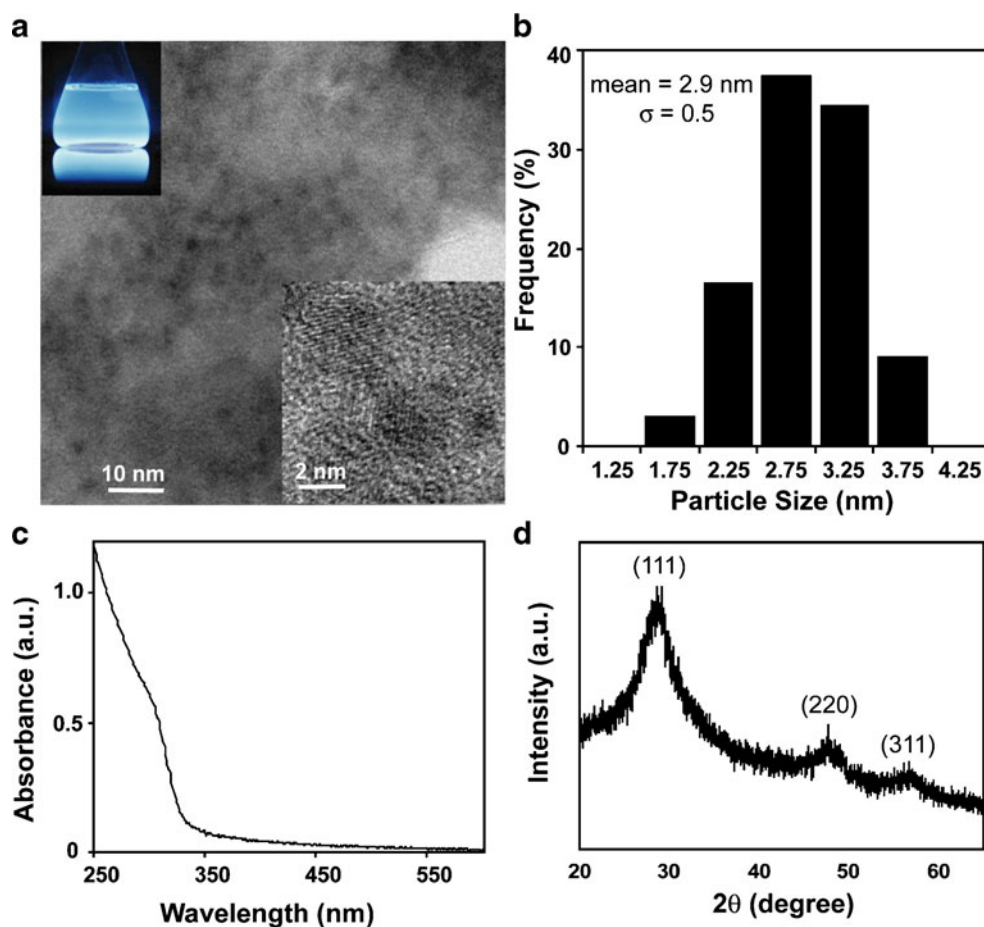

Fig. 2 TEM image of Ag NPs with corresponding particle size distribution and SAED pattern (*inset*)

quenching in the present study [37]. Additionally, positive deviation (concave toward Y-axis) in the Stern–Volmer plot was observed at higher NP concentration. This superlinear behavior indicates the presence of mixed quenching [28] in the present system.

Due to strong surface complexation with citrate, surface of the Ag NPs prepared in the present study is negatively charged [36, 38]. Chitosan-stabilized ZnS QDs, on the other hand, are positively charged as the pK_a value of the chitosan amino group is estimated to be at ~6.3 [39]. The quenching of ZnS QDs by Ag NPs may arise from the formation of static quenching complex via attractive electrostatic interaction. In order to investigate this electrostatic interaction, UV-visible spectra of the Ag NPs in presence and absence of ZnS QDs were examined (Fig. 4a). Figure 4a clearly shows the simultaneous damping and broadening of the SPR band of Ag NPs in presence of ZnS QDs. This indicates the aggregation of Ag NPs in presence of ZnS QDs. The electrostatic interaction between chitosan-stabilized ZnS QDs and Ag NPs may lead to the formation of a QD–NP ensemble where a single Ag NP can quench a large number of ZnS QDs. This effect in turn could result in the extraordinary quenching efficiency observed here. The formation of

electrostatic complex during the quenching process was further supported by the observation that the increase in ionic strength significantly reduces the quenching efficiency [37, 40]. Figure 4b shows the regaining of fluorescence from Ag NP-quenched ZnS QDs upon addition of salt (NaCl). This observation was consistent with the previous reports of reduced quenching efficiency due to ionic screening [37].

However, the positive deviation of the Stern–Volmer plot indicates that additional mechanisms, in conjunction with electrostatic complex formation, are involved [28, 37] in the quenching of ZnS QD fluorescence by Ag NPs. The involvement of energy transfer and electron transfer mechanism in the interacting QD–NP pair has already been reported. Electron transfer mechanism which is only predominant in smaller (<5 nm) metal nanoparticles [41] does not seem to play significant role as the Ag NPs in the present study are much larger (~37 nm). On the other hand, energy transfer may significantly influence the present
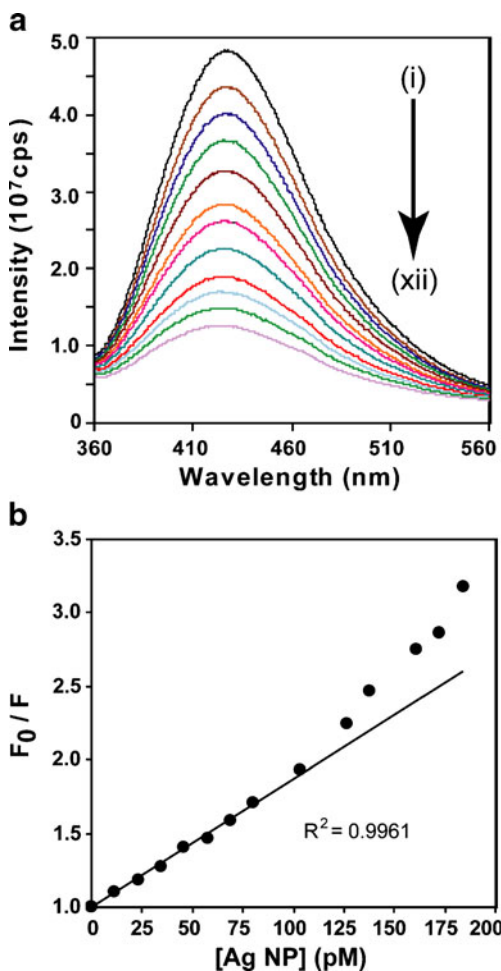
Fig. 3 **a** Fluorescence of chitosan capped ZnS QDs (1.4 μM) in presence of (1) 0, (2) 11.5, (3) 2.30, (4) 3.45, (5) 4.60, (6) 6.90, (7) 8.05, (8) 10.35, (9) 12.65, (10) 13.8, (11) 16.1, and (12) 18.4 pM Ag NPs. **b** Stern–Volmer plot of the corresponding fluorescence quenching
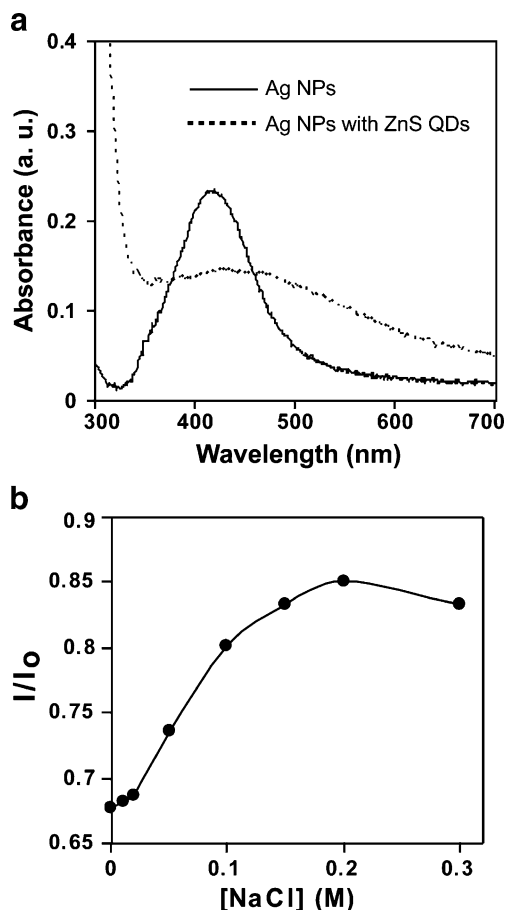

Fig. 4 **a** Absorption spectra of Ag NPs (11.5 pM) in the presence and absence of ZnS QDs (1.4 μM). **b** The fluorescence recovery of ZnS QDs on addition of varying concentration of NaCl. Io and I are the integrated fluorescence intensity of QDs in absence and presence of Ag NPs, respectively

quenching process due to the excellent overlap between ZnS QDs emission and the SPR band of Ag NPs (Fig. 5).

FRET can be defined as a process in which the excited-energy from the initially excited "donor" molecule is transferred to an "acceptor" molecule. FRET occurs without the appearance of a photon and is a result of long-range dipole–dipole interactions between the "donor" and "acceptor" [28]. In the present study, ZnS QDs and Ag NPs act as "donor" and "acceptor", respectively. The rate of energy transfer depends upon (1) the extent of spectral overlap between the donor emission and the acceptor absorption, (2) the relative orientation of the transition dipole of the donor and the acceptor, (3) the distance between the donor and the acceptor, and (4) the quantum yield of the donor [28]. The Förster distance R_o, defined as the distance at which resonance energy transfer is 50% efficient, is given by:

$$R_o = [8.8 \times 10^{-25} \kappa^2 n^{-4} \varphi J]^{\frac{1}{6}} \text{ (in centimeters)} \qquad (3)$$
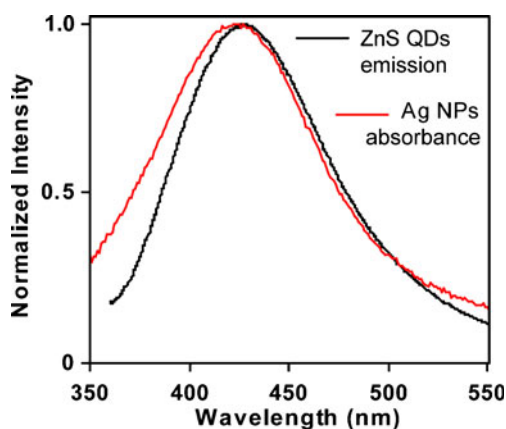
Fig. 5 Spectral overlap between the emission of ZnS QDs and absorbance of Ag NPs

Fig. 6 Fluorescence decay profile of ZnS QDs in absence and presence of Ag NPs

where κ^2 is the orientation factor between the emission dipole of the donor and the absorption dipole of the acceptor, n is the refractive index of the medium, ϕ is the quantum yield of the donor in absence of acceptor, and J(λ) is the overlap integral of the fluorescence emission spectra of the donor and the absorption spectra of the acceptor in units of $M^{-1}cm^3$. J(λ) is given by [28]

$$J(\lambda) = \int_0^\infty F_D(\lambda)\, \varepsilon_A(\lambda) \lambda^4 d\lambda \qquad (4)$$

where, $F_D(\lambda)$ is the corrected fluorescence intensity of the donor with total intensity normalized to unity, $\varepsilon_A(\lambda)$ is the decadic extinction coefficient of the acceptor at λ, which is in unit of $M^{-1}cm^{-1}$. In the present case, $\varphi = 0.095$, $n = 1.33$, $\kappa^2 = 2/3$. According to Eqs. (3) and (4), values of the above parameters were found to be $J = 2.2 \times 10^{-9} M^{-1} cm^3$ and $R_o = 18.4$ nm. The value of R_o is higher than the conventional Förster distance which could be due to large size and higher molar extinction coefficient of Ag NPs. This also indicates the involvement of NSET process [42].

Were the energy transfer between the excited ZnS QDs and Ag NPs responsible for emission quenching, characteristic signature can be found in the emission decay profile of the ZnS QDs in time-resolved fluorescence measurements [43, 44]. Time-correlated single-photon counting provides an accurate measurement of energy transfer, excluding both ground-state complex formation and inner filter effect. Figure 6 shows the emission decay of ZnS QDs at 427 nm both in presence and absence of Ag NPs. The resulting fluorescence can be fitted to exponential curve in order to derive the decay time constants, which can be used to calculate the lifetime of the fluorophore. It is evident from Fig. 6 that ZnS QDs follows a multi-exponential decay, characteristic of semiconductor QDs [45]. The decay was analyzed using biexponential kinetics
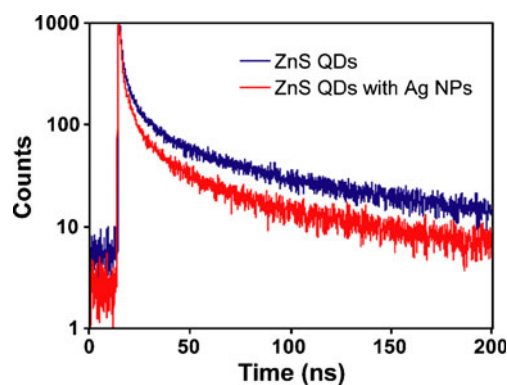
$$I(t) = \sum_i \alpha_i \exp(-t/\tau_i) \qquad (5)$$

where, α_i and τ_i are the pre-exponential factors and excited-state fluorescence lifetimes associated with the ith component, respectively. The lifetimes (τ_1 and τ_2) and pre-exponential factors (α_1 and α_2) of ZnS QDs emission at different Ag NPs concentration, is summarized in Table 1. For the biexponential decay the average lifetime$<\tau>$was determined from the equation [28]

$$<\tau> = \sum_i \frac{\alpha_i \tau_i^2}{\alpha_i \tau_i} \qquad (6)$$

ZnS nanocrystal show an average lifetime of 47.05 ns in the absence of Ag NPs, which decreases with increase in Ag NPs concentration due to the availability of more number of acceptors. The decrease in average lifetime of the ZnS QDs confirms the involvement of an additional mode of quenching, other than Coulombic interaction, possibly through energy-transfer process between the ZnS QD—Ag NP pair. Moreover, this explains the positive deviation observed in the Stern–Volmer plot.

Table 1 Life-time data obtained using the biexponential model for the ZnS QDs in absence and presence of Ag NPs

AgNPs/ ZnSQDs	α_1	τ_1 (ns)	α_2	τ_2 (ns)	$<\tau>$ (ns)	χ^2
0	117	7.55	73.5	55.6	47.05	1.08
1.66×10^{-5}	129	6.60	66.8	52.45	43.65	1.07
3.32×10^{-5}	106.2	6.37	48.4	44.42	35.31	1.09
4.98×10^{-5}	205.3	4.67	53.8	42.89	31.68	1.14

Conclusion

In summary, water dispersible chitosan-stabilized ZnS QDs of ca. 3 nm were prepared in an environment friendly method. The interaction of ZnS QDs with citrate-capped Ag NPs resulted in the fluorescence quenching of the QDs in concentration-dependent manner. The corresponding Stern–Volmer plot for the present fluorophore–quencher pair indicated mixed nature of quenching with a high K_{sv} value (9×10^9 M^{-1}) which demonstrates the efficient quenching of ZnS QDs by Ag NPs. The Coulombic interaction between the positively charged ZnS QDs and negatively charged Ag NPs led to the formation of electrostatic complex that contribute to the static mechanism of the quenching process. Furthermore, the involvement of energy transfer process due to excellent spectral overlap between ZnS QDs emission and SPR band of Ag NPs was confirmed by the time-resolved fluorescence measurements. The R_o value calculated for the present donor-acceptor pair was found to be 18.4 nm which was greater than the generally observed Förster distance. The implication of the present findings may lead to the development of long-range FRET- or NSET-based methods for studying biological multi-component system.

References

1. Zhong W (2009) Nanomaterials in fluorescence-based biosensing. Anal Bioanal Chem 394:47–59
2. Alivisatos AP (1996) Perspectives on the physical chemistry of semiconductor nanocrystals. J Phys Chem 100:13226–13239
3. Smith AM, Ruan G, Rhyner MN, Nie S (2006) Engineering luminescent quantum dots for in vivo molecular and cellular imaging. Anal Biomed Eng 34:3–14
4. Medintz IL, Uyeda HT, Goldman ER, Mattoussi H (2005) Quantum dot bioconjugates for imaging, labelling and sensing. Nat Mater 4:435–446
5. Han M, Gao X, Su JZ, Nie S (2001) Quantum-dot-tagged microbeads for multiplexed optical coding of biomolecules. Nat Biotechnol 19:631–635
6. Alviastos P (2004) The use of nanocrystals in biological detection. Nat Biotechnol 22:47–52
7. Jamieson T, Bakhshi R, Petrova D, Pocock R, Imani M, Seifalian AM (2007) Biological applications of quantum dots. Biomaterials 28:4717–4732
8. Li X, Qian J, Jiang L, He S (2009) Fluorescence quenching of quantum dots by gold nanorods and its application to DNA detection. Appl Phys Lett 94:063111–063113
9. Dyadyusha L, Yin H, Jaiswal S, Brown T, Baumberg JJ, Booy FP, Melvin T (2005) Quenching of CdSe quantum dot emission, a new approach for biosensing. Chem Commun 25:3201–3203
10. Willard DM, Orden AV (2003) Quantum dots: resonant energy-transfer sensor. Nat Mater 2:575–576
11. Medintz IL, Clapp AR, Mattoussi H, Goldman ER, Fisher B, Mauro JM (2003) Self-assembled nanoscale biosensors based on quantum dot FRET donors. Nat Mater 2:630–638
12. Ray K, Badugu R, Lakowicz JR (2006) Metal-enhanced fluorescence from CdTe nanocrystals: a single-molecule fluorescence study. J Am Chem Soc 128:8998–8999
13. Dulkeith E, Ringler M, Klar TA, Feldmann J, Javier AM, Parak WJ (2005) Gold nanoparticles quench fluorescence by phase induced radiative rate suppression. Nano Lett 5:585–589
14. Murgadoss A, Chattopadhyay A (2008) Tuning photoluminescence of ZnS nanoparticles by silver. Bull Mater Sci 31:533–539
15. Zhang J, Fu Y, Chowdhury MH, Lakowicz JR (2007) Metal-enhanced single-molecule fluorescence on silver particle monomer and dimer: coupling effect between metal particles. Nano Lett 7:2101–2107
16. Pompa PP, Martiradonna L, Torre AD, Sala FD, Manna L, Vittorio MD, Calabi F, Cingolani R, Rinaldi R (2006) Metal-enhanced fluorescence of colloidal nanocrystals with nanoscale control. Nat Nanotechnol 1:126–130
17. Aslan K, Gryczynski I, Malicka J, Matveeva E, Lakowicz JR, Geddes CD (2005) Metal-enhanced fluorescence: an emerging tool in biotechnology. Curr Opin Biotechnol 16:55–62
18. Aslan K, Lakowicz JR, Geddes CD (2005) Metal-enhanced fluorescence using anisotropic silver nanostructures:critical progress to date. Anal Bioanal Chem 382:926–933
19. Sabatini CA, Pereira RV, Gehlen MH (2007) Fluorescence modulation of acridine and coumarin dyes by silver nanoparticles. J Fluoresc 17:377–382
20. Nabika H, Deki S (2003) Enhancing and quenching functions of silver nanoparticles on the luminescent properties of europium complex in the solution phase. J Phys Chem B 107:9161–9164
21. Tay LL, Rowell N, Boukherroub R (2005) Colloidal silver nanoparticle induced photoluminescence quench on the surface functionalized planar si. Mater Res Soc 901:221
22. Umadevi M, Vanelle P, Terme T, Rajkumar BJM, Ramakrishnan V (2009) Fluorescence quenching of 1, 4-Dihydroxy-2, 3-Dimethyl-9, 10-anthraquinone by silver nanoparticles: size effect. J Fluoresc 19:3–10
23. Zhang J, Fu Y, Chowdhury MH, Lakowicz JR (2007) Enhanced Förster resonance energy transfer on single metal particle. 2. dependence on donor−acceptor separation distance, particle size, and distance from metal surface. J Phys Chem C 111:11784–11792
24. Yun CS, Javier A, Jennings T, Fisher M, Hira S, Peterson S, Hopkins B, Reich NO, Strouse GF (2005) Nanometal surface energy transfer in optical rulers, breaking the FRET barrier. J Am Chem Soc 127:3115–3119
25. Saini S, Bhowmick S, Shenoy VB, Bagchi B (2007) Rate of excitation energy transfer between fluorescent dyes and nanoparticles. J Photochem Photobiol A Chem 190:335–341
26. H. C. Warad, C. Thanachayanont, G. Tumcharern, J. Dutta, (2007) Proceedings of the 2nd IEEE International Conference on Nano/Micro Engineered and Molecular System; Bangkok Thailand.
27. Williams ATR, Winfield SA, Miller JN (1983) Relative fluorescence quantum yields using a computer-controlled luminescence spectrometer. Analyst 108:1067–1071
28. Lakowicz JR (1999) Principles of fluorescence spectroscopy, 3 rdth edn. Kluwer/Plenum, New York
29. Turkevich J, Stevenson PC, Hillier J (1951) A study of the nucleation and growth processes in the synthesis of colloidal gold, John Turkevich Discuss. Faraday Soc 11:55–75
30. Xiao Q, Xiao C (2008) Synthesis and photoluminescence of water-soluble Mn^{2+}-doped ZnS quantum dots. Appl Surf Sci 254:6432–6435
31. Lippens PE, Lannoo M (1989) Calculation of the band gap for small CdS and ZnS crystallites. Phys Rev B 39:10935–10942

32. Brus L (1986) Electronic wave functions in semiconductor clusters: experiment and theory. J Phys Chem 90:2555–2560

33. Mall M, Kumar L (2010) Optical studies of Cd^{2+} and Mn^{2+} Co-doped ZnS nanocrystals. J Lumin 130:660–665

34. Sapra S, Prakash A, Ghangrekar A, Periasamy N, Sarma DD (2005) Emission properties of manganese-doped ZnS nanocrystals. J Phys Chem B 109:1663–1668

35. Pillai ZS, Kamat PV (2004) What factors control the size and shape of silver nanoparticles in the citrate ion reduction method. J Phys Chem B 108:945–951

36. Puebla RAA, Aroca RF (2009) Synthesis of silver nanoparticles with controllable surface charge and their application to surface-enhanced Raman scattering. Anal Chem 81:2280–2285

37. Fan C, Wang S, Hong JW, Bazan GC, Plazco KW, Heeger AJ (2003) Beyond superquenching: hyper-efficient energy transfer from conjugated polymers to gold nanoparticles. PNAS 100:6297–6301

38. Longa D, Wua G, Chen S (2007) Preparation of oligochitosan stabilized silver nanoparticles by gamma irradiation. Radiat Phys Chem 76:1126–1131

39. Tan WB, Huang N, Zhang Y (2007) Ultrafine biocompatible chitosan nanoparticles encapsulating multi-coloured quantum dots for bioapplications. J Colloid Interface Sci 310:464–470

40. O'Connella MJ, Chana CK, Lia W, Hicksa RK, Doorna SK, Wang HL (2007) Polyelectrolyte platform for sensitive detection of biological analytes via reversible fluorescence quenching. Polymer 48:7582–7589

41. Ghosh SK, Pal A, Kundu S, Nath S, Pal T (2004) Fluorescence quenching of 1-methylaminopyrene near gold nanoparticles: size regime dependence of the small metallic particles. Chem Phys Lett 395:366–372

42. Griffin J, Singh AK, Senapati D, Rhodes P, Mitchell K, Robinson B, Yu E, Ray PC (2008) Size- and distance-dependent nanoparticle surface-energy transfer (NSET) method for selective sensing of hepatitis C virus RNA. Chem Eur J 15:342–351

43. Sarkar S, Bose R, Jana S, Jana NR, Pradhan N (2010) Doped semiconductor nanocrystals and organic dyes: an efficient and greener FRET system. J Phys Chem Lett 1:636–640

44. Huang F, Lerner E, Sato S, Amir D, Haas E, Fersht AR (2009) Time-resolved fluorescence resonance energy transfer study shows a compact denatured state of the B domain of protein A. Biochemistry 48:3468–3476

45. Williams G, Kamat PV (2009) Graphene–semiconductor nanocomposites: excited-state interactions between ZnO nanoparticles and graphene oxide. Langmuir 25:13869–13873